

Published in IET Communications
 Received on 17th February 2009
 Revised on 1st June 2009
 doi: 10.1049/iet-com.2009.0117



Characterisation of a time-variant wireless propagation channel for outdoor short-range sensor networks

S. Wyne¹ T. Santos¹ A.P. Singh² F. Tufvesson¹ A.F. Molisch³

¹Department of Electrical and Information Technology, Lund University, Box 118, SE-221 00 Lund, Sweden

²ST-Ericsson AB, Nya Vattentornet, SE-221 83 Lund, Sweden

³Department of Electrical Engineering, University of Southern California, 3740 McClintock Avenue, Los Angeles, CA 90089-2565, USA

E-mail: shurjeel.wyne@eit.lth.se

Abstract: This study presents sample measurements and analysis characterising the radio channel for outdoor short-range sensor networks. A number of transmit and receive antennas are placed on the ground in an open area. The measured propagation channel is time varying because of the controlled motion of a person walking in the vicinity of the nodes. The statistics of both the line-of-sight (LOS) path and the scattered component of the measured channel are observed to be non-stationary. The channel (power) gains are found to be significantly influenced by the pedestrian movement, only when the LOS path is momentarily blocked. The authors present a generic approach to model receive signal fluctuations because of body blockage of the LOS path. Our approach, which is similar to the referenced work of Pagani and Pajusco, additionally models the time-variant Doppler spectrum of the residue (scattered) component of the measured channel, that is the remainder of the measured channel after the LOS path has been extracted. The proposed modelling approach is parameterised and validated from the measurements.

1 Introduction

Wireless sensor and *ad hoc* networks, where nodes communicate without fixed infrastructure, have been a very active research topic in recent times (see e.g. [1–3], and references therein). Outdoor short-range (inter-node distance less than 10 m) sensor networks are of interest for surveillance, environmental monitoring and communications applications. The scenario most relevant for practical applications has the nodes at fixed positions near the ground, so that temporal variations occur only because of people/objects moving in the vicinity of the sensors.

As one of the first and most fundamental steps, the wireless propagation channel for such networks needs to be characterised in order to determine performance limits in terms of capacity, reliability, energy consumption and latency. As an example, the amount of cooperation required between nodes to achieve a certain outage probability is

determined by the fading statistics between pairs of sensor nodes [4]. The channel characteristics, in turn, depend on the environment in which the sensor networks are operating. When one of the nodes is moving, changes in the spatial fading pattern are responsible for the temporal variations of the channel. In contrast, for fixed-node wireless links the channel is time variant because of motion of scatterers in the vicinity of the nodes.

When a human pedestrian walks in the vicinity of a link, the received signal experiences fading. This fading may be because of the pedestrian's body blocking (absorbing) the signal or the fluctuations may be because of interference from multipath components that are diffracted or scattered off the pedestrian's body. In this work, the term scattering will be used both for specular reflection and interaction of electromagnetic waves with rough surfaces. Independent investigations of propagation in the 2.4 GHz ISM band have revealed that the human body may be modelled by a

homogeneous lossy medium with relative permittivity, $\epsilon_r = 53.5$ and conductivity, $\sigma_c = 1.81$ S/m, which are representative of muscle tissue [5, 6]. With those electrical properties a transverse electric polarised wave at 2.6 GHz may experience reflection coefficients on the order of 0.76–1, when reflected off the pedestrian's body.

To the best of the authors' knowledge, fixed-sensor outdoor channels have not been investigated in detail in the literature. Although there is a rich literature on cellular-type outdoor channels [7], cellular transmitters are high above the ground, and thus are significantly different from the scenario we are interested in. Peer-to-peer outdoor communications are usually characterised by the fact that at least one of the devices is moving. Furthermore, transceivers are still considerably higher above the ground than in outdoor sensor networks. Several investigations, for example [8–10] have measured or modelled outdoor propagation between sensors close to the ground, but did not investigate temporal variations because of moving scatterers. Furthermore, they concentrated on much larger distances between the sensors. The scenarios in [11–13] are closest to the ones we are interested in for this paper, in that they measured and modelled temporal variations of the channel because of moving scatterers and in particular considered the effect of people moving through the line-of-sight (LOS). However, those investigations were done in indoor environments.

In this paper we present results for the time-variant narrowband fading statistics from an outdoor measurement campaign where the nodes were static and a person was walking in the vicinity of the nodes. Although the number of measurements is not sufficient for a statistically reliable parameterisation of a model, we can gain qualitative insights into the most important phenomena. The measurements were performed at 2.6 GHz, which is close enough to the 2.45 GHz ISM band to yield similar propagation results, but separated enough that the measurements did not suffer from interference. The antennas, also referred to as nodes, were placed outdoors on the ground, and arranged in a topology consisting of two parallel rails.

We discuss qualitative effects on the received signal when a person is walking between the rails, particularly when the LOS path is blocked because of this motion. The LOS path, in this work, is defined as the first-arriving component in the channel impulse response (CIR). We present a generic approach to model temporal variations of the received signal strength, arising from a temporary blockage of the LOS path. Our approach has some features common with the method presented in [11]. However, our analysis has the following salient differences:

- We investigate the narrowband case of LOS blockage by a pedestrian, that is in addition to characterising fading of the first-arriving path, which is extracted from measurements, the fading of the residue (scattered) component of the

measured channel, that is the remainder after the LOS path has been extracted, is also investigated.

- The contribution of the dominant component is extracted differently.
- The measured scenario is outdoors and consequently the number of significant stationary scatterers is substantially smaller than in a typical indoor environment.
- Multiple links are measured jointly on the rails as opposed to point-to-point communication links characterised in [11].

It is important to note that the channel statistics are non-stationary, as will be reflected in the model we derive from the measurements.

The remainder of the paper is organised as follows: the measurement setup and post-processing are described in Section 2, Section 3 contains the results and discussion. Finally, the paper is concluded in Section 4.

2 Measurement setup and processing

2.1 Equipment

The channel transfer functions between different sensor nodes were recorded with the RUSK Lund wideband channel sounder that measures the transfer functions by means of a multicarrier signal [14]. Fast radio frequency (RF) multiplexers are used at the transmit (Tx) and receive (Rx) side to sequentially connect antenna elements to a common RF chain at respective side.

The measurements were performed at a centre frequency of 2.6 GHz and a transmission bandwidth of 200 MHz, spanned by 321 subcarriers (tones). Each of these tones has the interpretation of a separate (possibly correlated) realisation of the narrowband channel characterised in this work; to verify the underlying assumption of frequency stationarity of the tones, magnitude fluctuations of the transfer function of each link were inspected, the fluctuations were observed to be insignificant over the measured bandwidth, thus validating the frequency stationarity assumption. The Tx signal used in the measurements had an output power of 27 dBm and was repeated with a period of 1.6 μ s. One cycle of measurements over all 36 Tx–Rx combinations, termed a channel snapshot, was completed in 134 μ s [$6 \times 7 \times 2 \times 1.6 \mu$ s] where additional guard periods were used for Tx and Rx switching to avoid measurement of switching transients.

To improve the measurement signal-to-noise ratio (SNR), which was on the order of 10 dB or more, each channel snapshot was accompanied by nine extra snapshots spaced a fraction of a μ s apart. This set of ten snapshots was vectorially averaged to provide a 10 dB improvement in SNR; in the very short time span needed to measure the

ten snapshot set the radio channel can be assumed static, so that only the random measurement noise changes realisations among these snapshots.

The temporal variations of the radio channel were tracked by recording the ten snapshot set at regular 10 ms intervals. This sampling rate of 100 Hz is in excess of the minimum requirement of twice the maximum Doppler frequency induced by normal walking speed (1.5 m/s) of the pedestrian. The total observation interval for each measurement record was 10 s.

The Tx and Rx antennas were commercial Skycross (SMT-2TO6MB-A) meander line antennas with a linear polarisation; when the major axis of the antenna's rectangular printed circuit board (PCB) is oriented vertically, the E_θ electric field component is the dominant polarisation. Furthermore, the pattern is omnidirectional in the azimuthal (horizontal) plane, although some lobes exist in the elevation plane. The antenna dimensions are $6 \times 3 \times 0.4 \text{ cm}^3$ [15].

2.2 Scenario

Channel measurements were performed outdoors in a level grassy field near the M-building at LTH campus, Lund, Sweden. The six Tx and six Rx antennas were fixed at the ground level; the major axis of each antenna PCB was oriented vertically with the top edge of the PCB set to a height of 0.105 m above the ground. As shown in Fig. 1, the antennas were arranged along two virtual lines (rails) parallel to each other. Measurements were performed with a test pedestrian walking between the rails and parallel to the orientation of the rails. The pedestrian maintained a normal walking speed of 1.5 m/s throughout a measurement run. The measurements were repeated with a spacing of 2, 4 and 8 m between the two rails. The measurements took place on a sunny day in late spring, as

such the grass and other vegetation were relatively free of moisture.

Post-measurement analysis revealed that only 18 of the 36 SISO channels were actually measured in each scenario. These measured channels correspond to the following Tx–Rx combinations: each of Rx elements 1, 2 and 3 received the signal emanating from each of the Tx elements 1, 3 and 5 ($3 \times 3 = 9$ channels), these nodes are shown by green triangles in Fig. 1. Similarly, each of Rx elements 4, 5 and 6 received the signals emanating from each of the Tx elements 2, 4 and 6 ($3 \times 3 = 9$ channels), and these nodes are shown by red circles in Fig. 1. The analysis presented in the remainder of the paper is based on these 18 links. Note that while most of these links have Tx and Rx nodes on opposite rails, the unique location of Tx6 and Rx6 nodes enables measurement of links with Tx and Rx nodes on the same rail. For the latter type of links, the LOS path is not blocked by the pedestrian walking between the rails.

2.3 Post processing

In the analysed measurements a consistent observation was that the channel (power) gain was significantly influenced by the pedestrian only when the pedestrian's body blocked the LOS path. Fig. 2 shows the simultaneous development, over time, of the Rx signal power for various links as the test pedestrian walks between the rails. The Rx power shown in the plots is averaged over tones for each link. The pedestrian's influence on Rx power is prominently visible for opposite-rail links, for example Tx1–Rx1 because the LOS path is blocked temporarily by the pedestrian. An interesting observation is that the Rx power is not just continuously attenuated but exhibits oscillations, so that the pedestrian can increase the signal strength. This can be explained by additional signal energy reaching the receiver after being reflected off the pedestrian's body, as long as the pedestrian does not block the LOS path. In contrast,

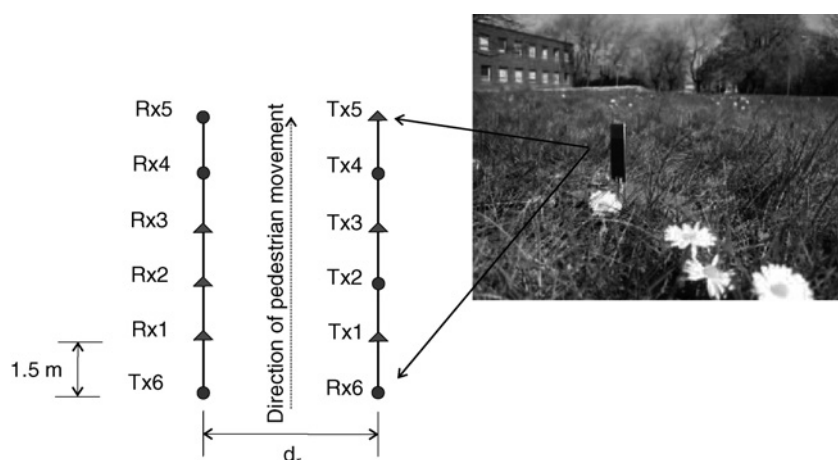


Figure 1 Measurement layout showing nodes placed on two parallel rails with adjustable rail widths, $d_r = 2, 4$ and 8 m

The pedestrian's walking path is also shown. Nodes that form communication pairs are highlighted by circles or triangles. The placement of one of the antennas in the grassy field is also shown

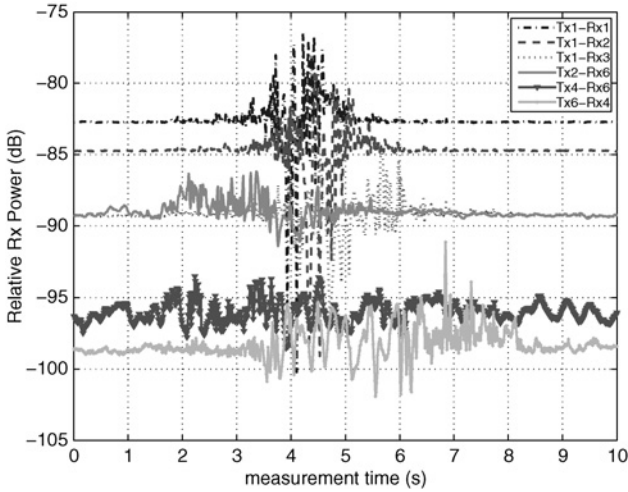


Figure 2 Fluctuations of relative Rx power on different links, as a pedestrian walks between the rails

The power has been averaged over all tones. The three solid-line curves represent links with Tx and Rx nodes on the same rail whereas the other three curves correspond to opposite-rail links. The plots are from a 2 m rail measurement

the same-rail links whose LOS path is not blocked by the pedestrian, exhibit no significant variations of the received power, for example refer to the Tx2–Rx6 link.

Besides the overall signal strength, we are interested in the properties of the LOS path only, and the residual channel (scattered components) only, that is the remainder of the measured channel after the LOS path has been extracted. Since the LOS component itself is time varying, it cannot be retrieved by the standard method of temporally averaging the measured complex channel gains. Instead, we perform the LOS identification in the delay domain, using the following approach: the CIR, $h_{i,j,\tau,l}$ is obtained by a fast Fourier transform (FFT) of the measured channel transfer function, $H_{i,j,k,l}$, as

$$h_{i,j,\tau,l} = \frac{1}{K} \sum_{k=0}^{K-1} H_{i,j,k,l} \exp\left(j2\pi \frac{k}{K} \tau\right) \quad (1)$$

where i, j, k and l denote Rx and Tx antenna, frequency and (temporal) snapshot index, respectively, the variable τ denotes delay bin index for the CIR and K is the number of measured tones. An improved estimate of the time delay of arrival of the LOS peak is obtained by interpolating the delay grid of the CIR with more samples in the inverse FFT than specified by K . The spacing between adjacent delay bins of the interpolated CIR is 0.05 ns as opposed to the 5 ns spacing achieved without interpolation. The interpolation allows plotting of the fine details of lobes of the different sinc (\cdot) functions in the CIR, each corresponding to a resolved multipath component. To achieve a narrow main-lobe peak, the FFT is applied with a rectangular window function. The complex gain of the

identified LOS path is then calculated as

$$\tau' = \arg \max_{\tau} (|h_{i,j,\tau,l}|^2) \quad (2)$$

$$\hat{h}_{i,j,\tau,l}^{\text{LOS}} = h_{i,j,\tau',l}$$

The LOS path's contribution to frequency domain, $H_{i,j,k,l}^{\text{LOS}}$, is subsequently estimated and removed from the measured channel, leaving behind the residue component of the measured channel, $H_{i,j,k,l}^{\text{Res}}$. The successful removal of the LOS component is verified by a null observed in the CIR for $H_{i,j,k,l}^{\text{Res}}$, at the delay of the removed peak. Note that $H_{i,j,k,l}^{\text{Res}}$ is to be distinguished from $H_{i,j,k,l}^{\text{LOS,Res}}$, where the latter is the random component within the extracted LOS path, and causes fading of the LOS path. The extraction of $H_{i,j,k,l}^{\text{LOS,Res}}$ will be discussed in Section 3.2.

Even when averaging out the small-scale fluctuations observed in Fig. 2, one can clearly see that the mean power of the Rx signal is time variant. Furthermore, as shown in Fig. 4 (details discussed in Section 3.1), the local average power of the LOS component also varies over the measurement duration. Therefore fading statistics can be considered as stationary only within a time window, that is a stationarity interval. The determination of stationarity intervals in our measurements could not be carried out using the method of [16] as it requires high-resolution channel parameter estimation; extension of this method to the distributed physical arrays under consideration is not straightforward. Another method proposed by [17] detects changes in the spatial structure of the channel by thresholding the change in correlation matrix of the multiple-input multiple-output (MIMO) channel. This too could not be applied since the spatial extent of the stationarity region that was to be determined, was on the order of the spatial extent of our distributed antenna arrays. Thus, temporal stationarity lengths for this work were investigated using the method of [18]; a local region of stationarity (LRS) was defined by a set of temporal snapshots where the correlation coefficient between consecutive averaged power delay profiles (APDPs) exceeded a pre-defined threshold of 0.5. The correlation coefficient is given by [18]

$$c(t_l, \Delta t) = \frac{\int \overline{P_b(t_l, \tau)} \overline{P_b(t_l + \Delta t, \tau)} d\tau}{\max\{\overline{P_b(t_l, \tau)}^2, \overline{P_b(t_l + \Delta t, \tau)}^2\}} \quad (3)$$

where $\overline{P_b(t_l, \tau)} = (1/N) \sum_{l=0}^{l+N-1} |h_{i,j,\tau,l}|^2$ is the averaged, and $P_b(t_l, \tau) = |h_{i,j,\tau,l}|^2$ is the instantaneous power delay profile (PDP), respectively. Furthermore, N is the number of PDPs to be averaged. The correlation coefficient in (3) is potentially influenced by (i) number of significant taps in the APDPs, (ii) averaging length, N , to remove small-scale fading and (iii) measurement noise. The suitability of this metric for our measurements was investigated through a simulation study employing stationary realisations of an exponential PDP. Noise was added to the realisations,

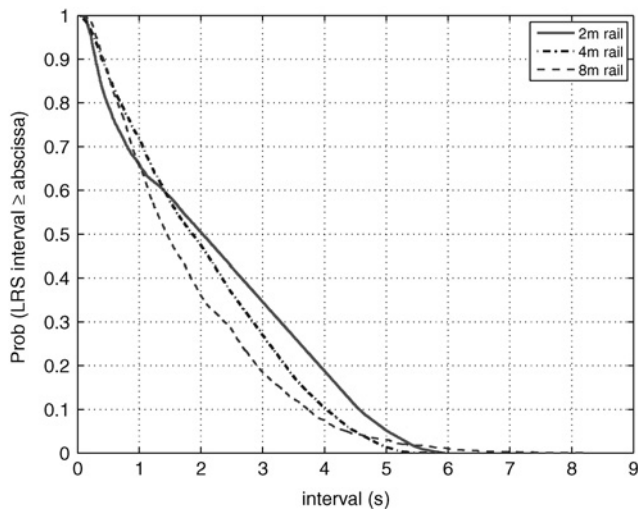


Figure 3 Empirical complementary cumulative distribution functions of LRS for different measurements

corresponding to SNR values in our measurements. It was observed that for $N \geq 40$ the correlation always exceeded the threshold, over an observation span corresponding to our measurements. In other words, the LRS metric gave the desired infinite duration of stationarity. Consequently, $N = 40$ was also selected for the measurements. Note that this figure is an obvious tradeoff; a larger window size increases the number of independent PDPs available for averaging, while the separability between small- and large-scale effects in the measurements benefits from a small window size. The LRS duration for different measurement scenarios is shown in Fig. 3. It can be observed that in 80–85% cases the channel can be considered stationary over a time interval of 0.5 s and measurement bandwidth of 200 MHz (relative bandwidth of around 7%). Consequently, a 0.5 s interval was considered as the temporal extent of a small-scale area (SSA).

The small-scale characteristics were investigated per single-antenna link. Within the 0.5 s wide-sense stationary window, the set of $H_{i,j,k,l}$ samples over the indices k and l were considered as a statistical ensemble. Furthermore, the window was slid over the measurement record length of 10 s to obtain small-scale characteristics in a continuous fashion. As a trade-off between processing time and continuous estimates of small-scale parameters, consecutive windows were set to have 80% overlap, that is the start point of a successive window was advanced by 11 temporal samples with respect to the start point of a preceding window, where a window length is 51 temporal samples.

3 Results

3.1 Qualitative behaviour of the LOS component

The received signal, its LOS component and its scattered components, all exhibit small-scale and large-scale fading

that is separated by appropriate signal processing. In this section, we describe the observed time-varying statistics of these fading processes. The presence of a person moving between the rails causes significant fluctuations, both increase and decrease, of the received signal power. Fig. 4 shows qualitative behaviour of signal variations over time; typical examples of the power contained in the LOS component, $H_{i,j,k,l}^{\text{LOS}}$, and the signal level averaged over the small-scale fading, $\sqrt{E_{l_{\text{SSA}}} [|H_{i,j,k,l}^{\text{LOS}}|^2]}$, are shown. In the latter expression, $E_{l_{\text{SSA}}} [\cdot]$ represents a windowed temporal average with a window-length set to the temporal extent of an SSA.

From Fig. 4 we can infer some qualitative results on the behaviour of the LOS path:

1. The extracted LOS path typically exhibits temporal fading, because of the presence of a random component. This is a consequence of finite system bandwidth. Within the delay resolution, leading to 1.5 m spatial resolution in our case, additional multipath components may not be distinguishable from the clean LOS path, and are extracted with it.
2. The LOS power is not affected unless the link is obstructed by the pedestrian, for example refer to Fig. 4d that shows fluctuations of Rx power on the Tx2–Rx6 link that has Tx and Rx nodes on the same rail.
3. The LOS obstruction by the pedestrian lasts for less than 1 s duration, though associated fluctuations typically last 3 s. This result is partly because (i) the obstructing pedestrian walks on a path approximately midway between the rails and parallel to the rails and (ii) the nodes are on the ground and are obstructed only by the leg-region of the pedestrian.
4. The moving average, over time, of power of the extracted LOS does not always exhibit a significant dip, for example compare Figs. 4a and 4b. This is, at least partly, because of incomplete separation of the small-scale and large-scale fading.
5. At large distance (8 m), obstruction of the LOS path does not cause any noticeable attenuation of the LOS power, for example refer to Fig. 4c. This is intuitively explained by the partial/minimal shadowing of the link when spatial extent of the pedestrian scatterer is small compared to the scatterer's distance to either link end.

Inferring from the above observations, for a communications link application [19, 20] the presence of the moving person can be neglected unless the LOS path is obstructed. For surveillance applications [19, 20], it appears that in that case, monitoring Rx power only would not be enough to detect a person in the envisioned scenarios; rather some small-scale fading parameters, for example the Ricean K -factor (K_{Rice}) may have to be monitored to detect an intruder.

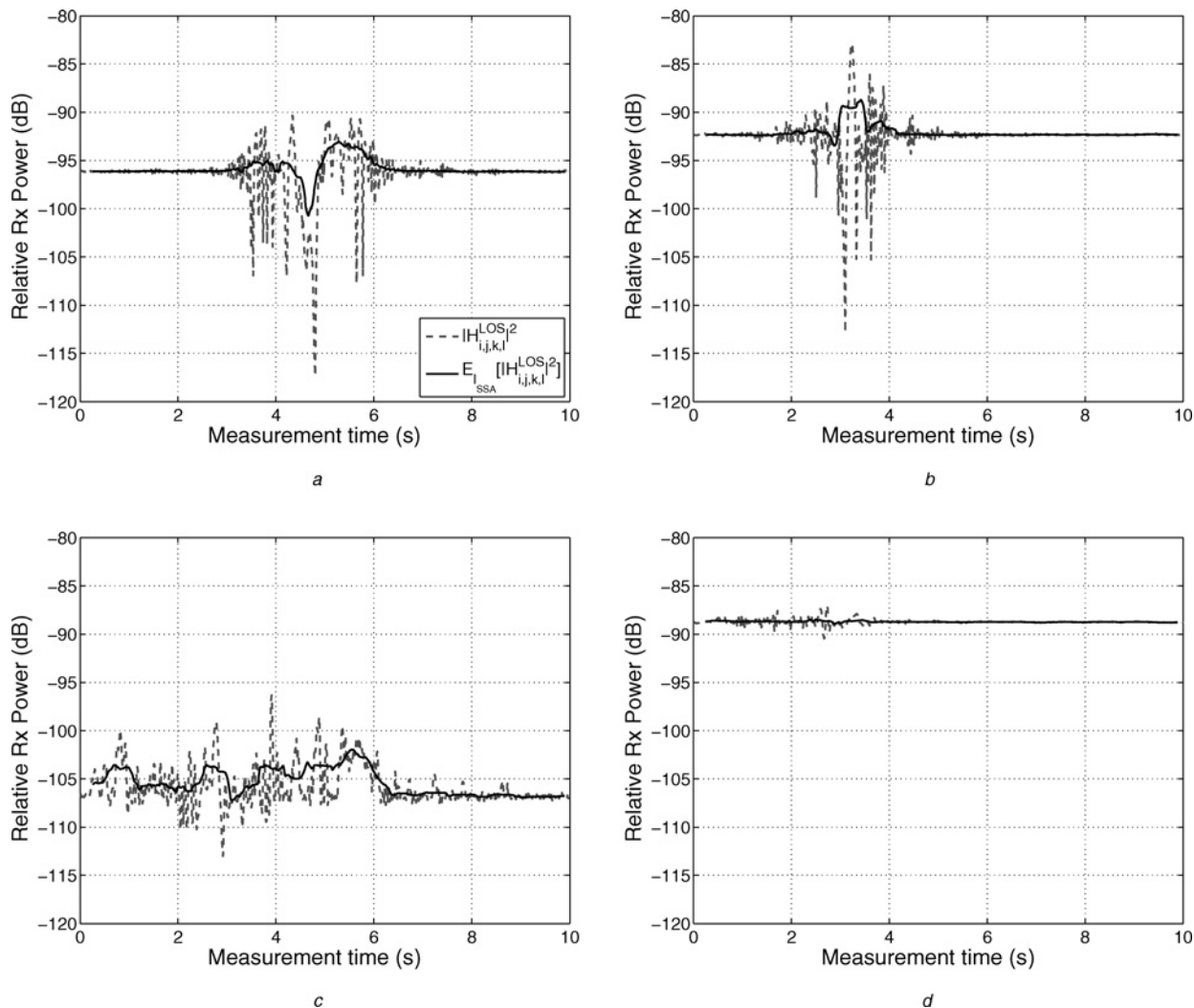


Figure 4 The pedestrian's influence on received power of $H_{i,j,k,l}^{LOS}$ (dashed curve), and local average of the power over time (solid curve). The measured links are indicated in the figure sub-captions

- a Tx5–Rx1 (4 m rail)
- b Tx1–Rx1 (4 m rail)
- c Tx1–Rx1 (8 m rail)
- d Tx2–Rx6 (4 m rail)

3.2 Large-scale statistics

From Fig. 4 one may observe that the local average power of the extracted LOS typically dips in level when the LOS path is shadowed by the pedestrian's body. There will be an associated change in the local average power of the LOS path's random component, $H_{i,j,k,l}^{LOS,Res}$. The latter component, though extracted with the clean LOS because of finite system bandwidth, can be separated in a post processing step written as

$$H_{i,j,k,l}^{LOS,Res} = \frac{H_{i,j,k,l}^{LOS}}{\sqrt{E_{l_{SSA}}[|H_{i,j,k,l}^{LOS}|^2]}} \quad (4)$$

In order to model power fluctuations of the LOS path, caused by body shadowing, it is proposed to characterise separately

the power of the deterministic mean, $\sqrt{E_{l_{SSA}}[|H_{i,j,k,l}^{LOS}|^2]}$, and the local average power of the random component, $H_{i,j,k,l}^{LOS,Res}$, of the extracted LOS path. For this purpose, we find that the model proposed in [11] for the indoor case works well in our scenario as well.

The power of the deterministic mean of the LOS path can be modelled, on a dB scale, by a Gaussian-shaped function, $g(t)$, written as [11]

$$g(t) = -A_S \left(1 - \left((t - t_0) \frac{2}{T_s} \right)^2 \right) \exp \left(-u \left((t - t_0) \frac{2}{T_s} \right)^2 \right) \quad (5)$$

where the parameter A_S represents shadowing attenuation, T_s is the shadowing duration, t_0 represents the shadowing instant, that is when the pedestrian blocks the LOS, and t is the observation time in seconds. Furthermore, the parameter u models the positive power gain at the edges of the large-scale fading pattern. This gain can be attributed to additional signal energy carried by reflections from the body when it is not blocking the LOS. In Figs. 4a and 4b, the LOS path is observed to experience a positive power gain on the order of 4–5 dB. These orders of magnitude are in line with an upper limit of +6 dB gain achievable in a theoretical two-path model with loss-less reflection and coherent summation of the paths.

Based on the 2 and 4 m rail measurements, recommended parameter values are: $A_S = 1-4$ dB, $T_s = 1$ s and $u \in [0.5, 1]$. For the case of the 8 m rail, the larger link distance results in minimal LOS blockage such that the temporal average of LOS power does not exhibit a dip. Therefore it is proposed to model the 8 m rail scenario by setting $A_S = 0$ in (5). It may be pointed out that our measurements were performed when the person was walking approximately in the middle between the two rails. Although the following case was not measured in our campaign, we conjecture that a person walking very close to either Tx or Rx node would result in power fluctuations even for the case of 8 m rail width.

The local average power of the LOS path's random component, $H_{i,j,k,l}^{LOS,Res}$, can be characterised in relation to the power of the LOS path's deterministic mean. This relative characterisation of the diffuse power is done in terms of the temporal Rice factors of the extracted LOS, $H_{i,j,k,l}^{LOS}$. For a small-scale ensemble of channel coefficients, K_{Rice} is determined by a grid-search for the value that maximises the likelihood of the ensemble being drawn from a Ricean probability distribution. The upper limit of the grid is based on the moment method [21] estimate of K_{Rice} , while the lower limit is set to zero.

The relative local average power of the diffuse component, $H_{i,j,k,l}^{LOS,Res}$, was found to be well represented, on a dB scale, by another Gaussian shaped function, $q(t)$, written with minor modifications to the original form [11] as

$$q(t) = A_{rel} + A_R \exp\left(-2\left((t - t_0)\frac{2}{T_R}\right)^2\right) \quad (6)$$

where A_{rel} is the dB power difference between the unobstructed LOS power and the mean power of the random component under the same conditions.

The values of the parameters were determined by a least-squares fit of the model to measured values: A_{rel} was typically within the range, -47 to -42 dB, for both the 2 and 4 m rail measurements. For the 8 m rail measurements, the larger link distance results in A_{rel} values around

-30 dB. The smaller K_{Rice} values for the 8 m rail measurements can be explained by the drop in the mean power of the deterministic component, compared to the power of the random component. The latter is the less affected of the two when the link distance is increased. Furthermore, the range of values for other parameters were: $A_R \in [38, 42]$ dB for the 2 and 4 m rails and $A_R \in [27, 29]$ dB for the 8 m rail. For the width of the bell-shaped curve, T_R is around 6 s for the 2 and 4 m rails and $T_R \in [8, 10]$ s for the 8 m rail. A sample curve for one of the measured links is shown in Fig. 5.

One may observe that the modelling approach for the power of the diffuse component works reasonably well.

3.3 Small-scale statistics

3.3.1 Envelope distribution: We first investigate the probability density function (PDF) of the narrowband case, using the Akaike information criteria (AIC) [22, 23]. The Rayleigh, Ricean, Nakagami-m, Weibull and lognormal distributions are considered as potential candidates for modelling the distribution of fading amplitudes. The maximum-likelihood estimates of these distribution parameters, as required by the AIC, were calculated for each small-scale ensemble; using closed-form expressions for Rayleigh and lognormal, grid-search for Ricean model, and results from [24, 25] for the Nakagami-m and Weibull distributions, respectively. The AIC favours the Ricean distribution in a majority of the cases covering different rail widths. Therefore the Ricean distribution is selected as a representative model for the fading amplitude distribution of the measured channel, $H_{i,j,k,l}$. To this effect, a representative distribution of the temporal K_{Rice} is shown for all 18 channels in Fig. 6.

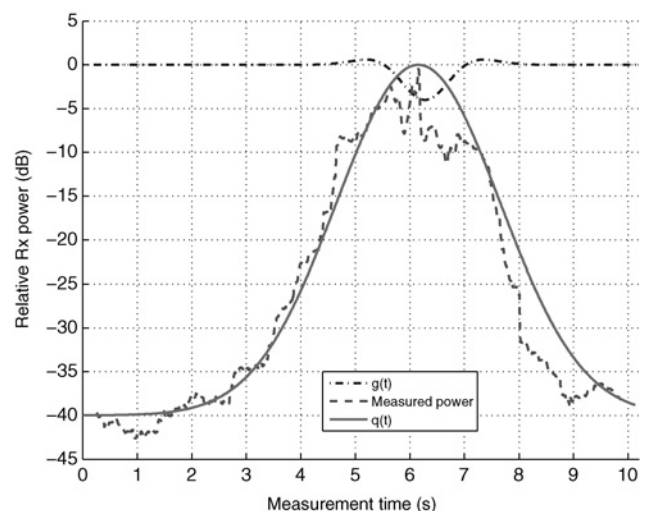


Figure 5 Measured local average power of $H_{i,j,k,l}^{LOS,Res}$ and its model, $q(t)$

The modelled power of the deterministic mean of LOS path, $g(t)$, is also shown. The pedestrian crosses the LOS path around 6.2 s. The plot corresponds to the Tx2–Rx5 link, measured in the 2 m rail scenario

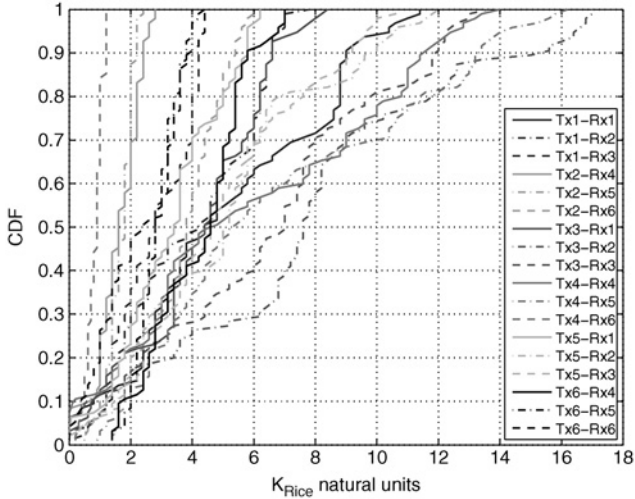


Figure 6 Distribution of temporal K_{Rice} for each of the 18 links, measured in the 4 m rail scenario

For the LOS path, a reliable determination of the appropriate PDF shape is not possible, because the small number of available samples (note that in the narrowband case, the different tones increase the size of the available statistical ensemble). But from heuristic reasoning, $H_{i,j,k,l}^{\text{LOS}}$ can also be assumed as Ricean, and its parameters determined from the measurements.

In addition to investigating the aggregate measured channel, its residue component, $H_{i,j,k,l}^{\text{Res}}$, was also investigated for the relevant fading amplitude distribution. Though the AIC determined the Ricean model as best fit in this case as well, the K -factors were quite small, $K_{\text{Rice}} \in [0, 1.5]$ natural units. In light of these observations, a Rayleigh process is proposed as an appropriate model for the fading distribution of the residue component of the measured channel, $H_{i,j,k,l}^{\text{Res}}$. Quantitative results for the power of this component are discussed in connection with its average Doppler spectrum in the next section.

3.3.2 Temporal correlation of small-scale fading:

The temporal correlation of small-scale fading, within a small-scale fading area, is a measure of how fast the channel changes in time, and is often characterised in terms of Doppler spectrum of the received signal [26]. The spectrum width is conventionally expressed in terms of the root-mean-square (RMS) Doppler-spread [26], σ_{dopp} , which can be estimated as

$$\sigma_{\text{dopp}} = \frac{\sum (f_i - f_m)^2 S(f_i)}{\sum S(f_i)} \quad (7)$$

where $S(f_i)$ is the power spectral density (PSD) at frequency shift, f_i , and $f_m = \sum f_i S(f_i) / \sum S(f_i)$ is the mean Doppler shift. The time-variant Doppler power spectrum for each link was generated by applying a short-time Fourier transform (STFT) to channel samples measured at each tone, and averaging the spectra over all tones to obtain the

link spectrum. The length of the STFT window was taken to be the 0.5 s stationarity interval.

The Doppler PSD of $H_{i,j,k,l}^{\text{LOS,Res}}$ characterises scattering of the extracted LOS component, and revealed a Laplacian shape (the Laplacian fit to the spectrum is not shown here because of space constraints) written as

$$S_{\text{LOS}}(f) = \frac{1}{\sqrt{2}\sigma_{\text{dopp}}} \exp\left(-\frac{\sqrt{2}}{\sigma_{\text{dopp}}}|f|\right) \quad (8)$$

The RMS Doppler spreads calculated according to (7) had values in the range, $\sigma_{\text{dopp}} \in [8, 12]$ Hz. These spreads are relatively large compared to those measured in indoor environments, (e.g. see [11]). However, the larger Doppler spreads are plausible because of a lack of significant stationary scatterers in the measured outdoor scenario. Since the moving person contributes a greater fraction of the total spectrum power compared to an indoor scenario, larger spreads follow. This reasoning was validated by performing indoor measurements with a similar setup; the measured spreads were on the order of 3 Hz.

The Doppler PSD of the random component, $H_{i,j,k,l}^{\text{Res}}$, characterises the spectral distribution of the residual power of the channel, after the LOS component has been removed. For the 2 and 4 m rail measurements, reflection off the person's body results in some distinct peaks in the Doppler spectrum, whereas for the 8 m rail measurements, no significant peaks were observed. Hence, in the sequel we discuss the spectrum only for the 2 and 4 m rail configurations.

Fig. 7 shows an example of the Doppler spectrum of a measured channel's random component, $H_{i,j,k,l}^{\text{Res}}$. The

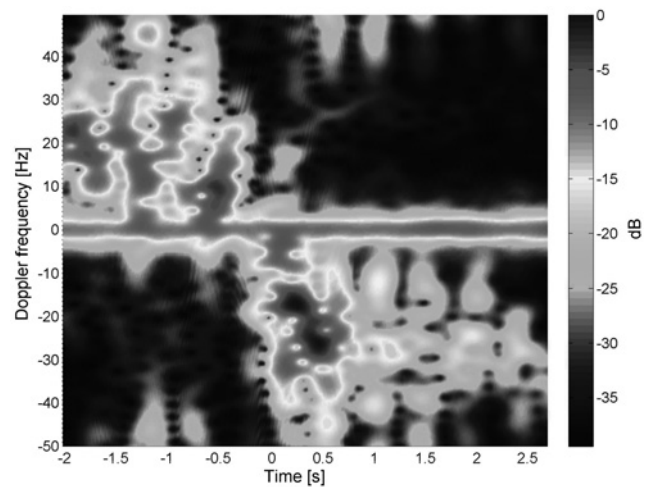


Figure 7 Doppler spectrum of the measured channel's random component, $H_{i,j,k,l}^{\text{Res}}$, for a typical link

The displayed spectrum corresponds to the Tx6-Rx6 link measured in the 2 m rail scenario. The time-axis is labelled relative to t_0 , which is at the origin

overall spectrum is observed to be time variant, though two distinct components can be identified:

1. A time-static component around 0 Hz, which is generated by reflections from stationary scatterers in the environment such as nearby buildings.
2. A time-variant component due to scattering off the pedestrian's body, which exhibits the strongest values when the person creates reflections close to the LOS crossing instant $t = t_0$; and weak power at the instant $t = t_0$, and towards the edges of the measurement interval.

On examining the Doppler spectra from different measurements, it was further confirmed that the power of the time-variant component of the spectrum was closely related to the un-obstructed LOS power, through the respective link distance. On the other hand, the power of the time-static component was observed to be independent of the link distance for the LOS path. The latter finding can be explained by the fact that the nearest building structures/trees were separated from the antennas by a distance on the order of a few tens of metres, which was much larger than the maximum LOS link distance in our measurements.

In general, the pattern of variations in the Doppler spectrum was quite similar for all the links with LOS blockage, therefore these link spectra were averaged to obtain a mean Doppler spectrum for further investigations of the pedestrian's effect. Prior to averaging, the time-static and time-variant components of each link's Doppler spectrum were separated by post-processing to allow different averaging techniques, whereas the time-static components of the Doppler spectra were averaged over the links without any weighting, the time-variant components were weighted and aligned prior to averaging. The weighting, based on respective un-obstructed LOS power, removed the distance-dependent power differences among

the dynamic spectra, and the alignment was performed at the time instant when the mean Doppler shift crossed 0 Hz, which also corresponded to the LOS crossing instant, t_0 .

In view of the common structure of measured spectra shown in Fig. 7, the Doppler spectrum was modelled, in natural units, as the sum of two Gaussian-shaped functions. The first of these functions, $D_s(t, f)$, centred at 0 Hz, represents the time-static component of the channel, while the second Gaussian curve, $D_p(t, f)$, represents the time-variant component of the channel due to the pedestrian. The latter curve is set to have a constant RMS Doppler spread of 15 Hz, calculated as the average of instantaneous RMS Doppler spreads observed over the 10 s measurement interval. Furthermore, $D_p(t, f)$ has a time-varying mean that goes through zero as the person passes through the LOS, and a time-varying strength (weak at 0, t_0 and 10 s, and strongest when the person creates reflections around t_0). At each time instant, the height (strength) of the $D_p(t, f)$ curve was adjusted to match the area under the curve, to the power of the measured average spectrum. The functional forms of these two Gaussian shapes with their parameters are provided in Table 1. Together, these relations can be used to model the temporal evolution of the non-stationary spectrum of $H_{i,j,k,l}^{\text{Res}}$.

It should be noted here that the expressions in Table 1 only model the Doppler spectral profile of $H_{i,j,k,l}^{\text{Res}}$; the power of $H_{i,j,k,l}^{\text{Res}}$ has to be related to LOS power through a scale factor. As stated previously, the power of the dynamic component, $D_p(t, f)$, is closely dependent on the link distance, that is the un-obstructed LOS power. Our analysis of measured spectra revealed that the ratio between un-obstructed LOS power and the peak (over time) power of the dynamic component was in the range of -2 to -6 dB. The dynamic component's power, obtained by integrating its PSD over frequency, peaked at the time instants T_1 and T_2 given in Table 1. On the other hand,

Table 1 Model for Doppler spectrum of $H_{i,j,k,l}^{\text{Res}}$

Symbol	Description	Function	Parameter	Unit
$D_p(t, f)$	pedestrian contribution	$p(t) \exp\left(-\frac{(f - f_m(t))^2}{2F_p^2}\right)$	$F_p = 12$	Hz
$p(t)$	Gaussian peak	$\exp\left(-\frac{(t - T_1)^2}{2W^2}\right) + \exp\left(-\frac{(t - T_2)^2}{2W^2}\right)$	$T_1 = -0.6$ $T_2 = 0.6$ $W = 0.32$	s s s
$f_m(t)$	mean Doppler	$-B \frac{2}{\pi} \text{atan}(Ct)$	$B = 22$ $C = 2.5$	Hz -
$D_s(t, f)$	time-invariant contribution	$\exp\left(-\frac{f^2}{2F_s^2}\right)$	$F_s = 1.4$	Hz

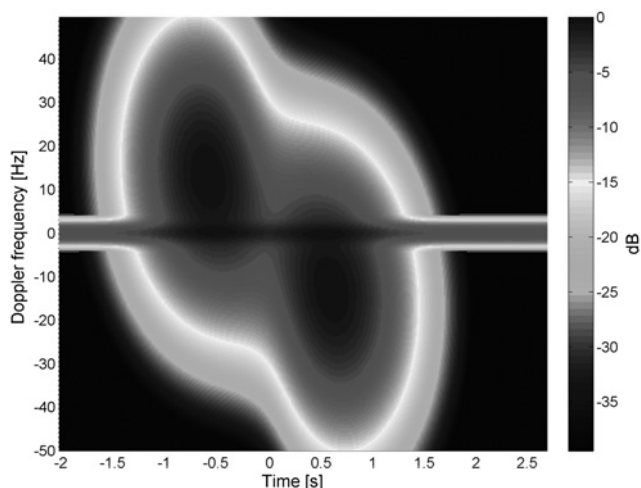


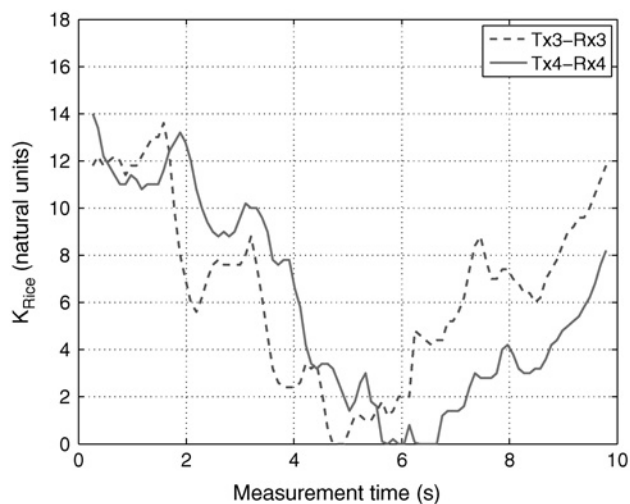
Figure 8 Modelled Doppler spectrum of the measured channel's random component, $H_{i,j,k,l}^{Res}$

The time axis is labelled relative to t_0 , which is at the origin

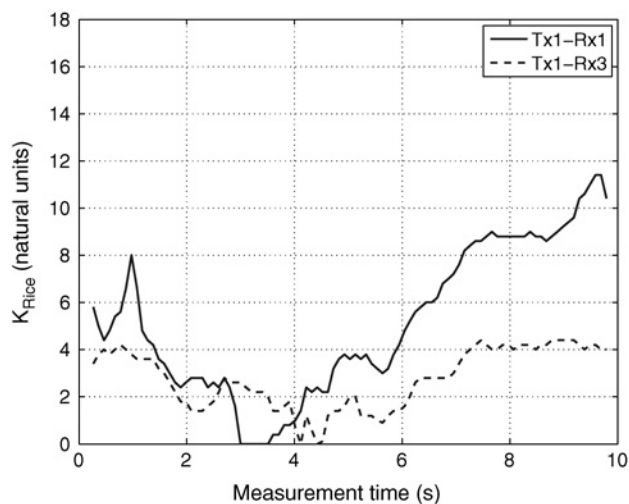
the power of the time-invariant component represented by $D_s(t, f)$, was independent of the LOS link distance, and related to the site geometry such as location of nearby buildings and trees. In our measurements, the power of the time-static component was observed to be -18 dB relative to the un-obstructed LOS power, when the antennas were exactly 2 m apart. The spectrum model generated by using Table 1 is shown in Fig. 8; the power of the static component in the model was set to -15 dB relative to peak power of the dynamic component of the modelled spectrum, this power difference was based on the measured spectrum shown in Fig. 7. One may observe that the model captures the essential pattern of variations in the measured Doppler spectrum of the link shown in Fig. 7.

3.4 Multi-channel characteristics

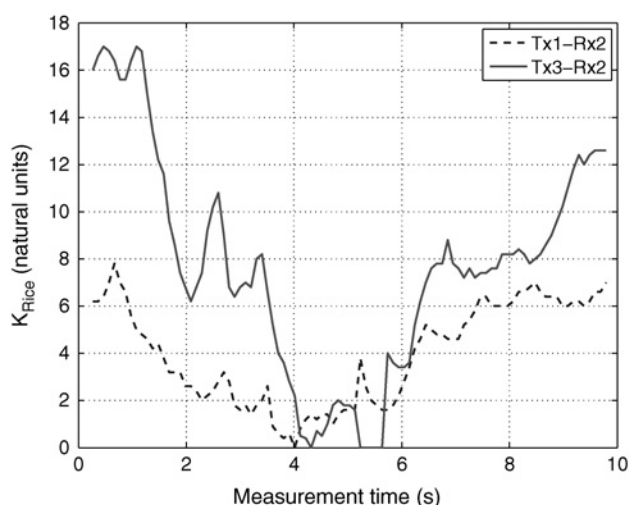
In sensor network applications, nodes may often be distributed over a spatial region in close proximity to one



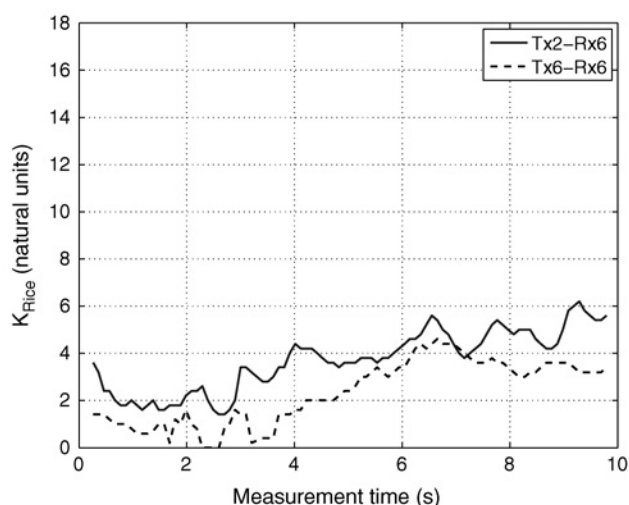
a



b



c



d

Figure 9 Evolution of temporal K_{Rice} at multiple link ends, as a pedestrian walks between the rails

The plots are taken from a 4 m rail measurement

another. It is of interest to observe, over time, the simultaneous influence of a scatterer's motion on the fading statistics at different spatial positions. Our measurements with nodes on parallel rails provide some useful insights on multi-channel characteristics, such as the correlation in temporal evolution of various links. Fig. 9 shows joint fading behaviour on different pairs of links. The plots show the temporal evolution of K_{Rice} on each link, as the pedestrian walks between the rails.

Some qualitative observations on the link correlations are now provided:

- Links that have similar orientation, relative to walking path of the pedestrian, have highly correlated fading statistics, see for example the links Tx3–Rx3 and Tx4–Rx4 in Fig. 9a.
- Consider two opposite-rail links that emanate from the same Tx, such as Tx1–Rx1 and Tx1–Rx3 shown in Fig. 9b: while K_{Rice} measured on the Tx1–Rx1 link increases in the interval between 4 and 5 s, K_{Rice} measured on Tx1–Rx3 link decreases during the same period. This behaviour is explained when one considers that the pedestrian is moving away from Rx1, during the 4–5 s period, so that the received time-variant component of the channel is gradually decreasing. Simultaneously, the pedestrian is getting closer to Rx3 such that the time-variant power, received at Rx3, from scattering/diffraction off the pedestrian's body is increasing. Since the temporal K_{Rice} , measured for stationary Tx/Rx, corresponds to a power ratio between the time-invariant component(s) of the channel and the components that are scattered/diffracted by a moving scatterer, the changes in the respective K_{Rice} follow.
- The link statistics are significantly correlated for the two opposite rail links, Tx1–Rx2 and Tx3–Rx2, which have transmitters spaced 3 m apart on the same rail, refer to Fig. 9c.
- Fig. 9d compares a same-rail link, Tx2–Rx6, with an opposite-rail link, Tx6–Rx6, that is spatially proximal and has approximately the same link distance. One observes that the time-variant scattering component is stronger for the opposite-rail link, resulting in a smaller K_{Rice} for the first 4 s of measurement time, that is the pedestrian passing that end of the rail. When the scattering/reflection component received off the pedestrian's body has diminished, the K_{Rice} values become similar for the two links.

It is noteworthy that all of the above effects describe the temporal correlation of the small-scale-averaged channel statistics; this is completely different from the standard MIMO correlation models, in which the correlation of instantaneous channel realisations is modelled [27].

4 Summary and conclusions

This paper presented a characterisation of an outdoor short-range sensor network scenario at 2.6 GHz. The terminals were stationary and placed at ground level on two parallel virtual rails. The channel was time variant because of a pedestrian walking between the rails. The influence of the pedestrian on Rx signal strength was most pronounced on the links where LOS blockage occurred because of body shadowing. On other links, specular/diffuse reflection off the person's body influenced the Rx signal strength, but to a lesser degree than the body-blockage case. An average stationarity interval of 0.5 s was established for the small-scale analysis. A narrowband characterisation of the channel was performed and the channel was observed to be Ricean fading. The measured RMS Doppler spreads were on the order of 10–15 Hz; these relatively high values, in comparison to similar indoor measurements, are because of a fewer number of significant stationary scatterers in the measured outdoor environment. A generic approach was presented to model temporally correlated samples of the narrowband channel. The time-variant Doppler spectrum of the residue channel was shown to have a distinct pattern associated with the pedestrian. These characteristics can be valuable for early intruder detection schemes since significant spectral peaks are visible before the LOS crossing instant. Furthermore, the sign on the Doppler shifts can be used to obtain information on the direction of movement of the intruder, a characteristic that cannot be extracted from the analysis of the LOS component only. Sample measurements on the link correlations were presented, which provide useful insight into the temporal evolution of joint fading behaviour of the links. Future measurements will focus on a similar characterisation for multiple people crossing the link with better tracking of their location during the measurement interval. Furthermore, a wider range of configurations for node placements will be considered to investigate the influence of geometry of movement.

5 Acknowledgments

This work was partly financed through the Swedish Foundation for Strategic Research, the High Speed Wireless Center at Lund University and a grant from Vetenskapsrådet, the Swedish Science Council. Part of this work was done while A.F. Molisch was at Mitsubishi Electric Research Labs, Cambridge, MA, USA and Lund University, Sweden, and A.P. Singh was at Lund University, Sweden.

6 References

- [1] GUTIÉRREZ J.A., CALLAWAY E.H., BARRETT R.L.: 'Low-rate wireless personal area networks: enabling wireless sensors with IEEE 802.15.4' (IEEE Press, 2003)

- [2] WILLIG A., MATHEUS K., WOLISZ A.: 'Wireless technology in industrial networks', *Proc. IEEE*, 2005, **93**, (6), pp. 1130–1151
- [3] HONG Y., HUANG W., CHIU F., KUO C.: 'Cooperative communications in resource-constrained wireless networks', *IEEE Signal Process. Mag.*, 2007, **24**, (3), pp. 47–57
- [4] MOLISCH A.F., MEHTA N., YEDIDIA J., ZHANG J.: 'Performance of fountain codes in collaborative relay networks', *IEEE Trans. Wirel. Commun.*, 2007, **6**, (11), pp. 4108–4119
- [5] VILLANESE F., SCANLON W.G., EVANS N.E.: 'Statistical characteristics of pedestrian-induced fading for a narrowband 2.45 GHz indoor channel'. Proc. IEEE VTC00-Fall, 2000, vol. 2, pp. 745–750
- [6] HALL P.S., HAO Y., NECHAYEV Y.I., ET AL.: 'Antennas and propagation for on-body communication systems', *IEEE Antennas Propag. Mag.*, 2007, **49**, (3), pp. 41–58
- [7] MOLISCH A.F., TUFVÉSSON F.: 'Multipath propagation models for broadband wireless systems' in IBNKAHLA M. (ED.): 'Digital signal processing for wireless communications handbook' (CRC Press, 2004, Ch. 2, pp. 2.1–2.43
- [8] ANDERSON C., VOLOS H., HEADLEY W., MULLER F., BUEHRER R.: 'Low antenna ultra wideband propagation measurements and modeling in a forest environment'. Proc. IEEE Wireless Communications and Networking Conf., 2008, pp. 1229–1234
- [9] SEE C., ABD-ALHAMEED R., HU Y., HOROSHENKOV K.: 'Wireless sensor transmission range measurement within the ground level'. Proc. Loughborough Antennas and Propagation Conf., 2008, pp. 225–228
- [10] MERRILL W., LIU H., LEONG J., SOHRABI K., POTTIE G.: 'Quantifying short-range surface-to surface communications links', *IEEE Antennas Propag. Mag.*, 2004, **46**, (3), pp. 36–46
- [11] PAGANI P., PAJUSCO P.: 'Characterization and modeling of temporal variations on an ultrawideband radio link', *IEEE Trans. Antennas Propag.*, 2006, **54**, (11), pp. 3198–3206
- [12] OESTGES C., VANHOENACKER-JANVIER D., CLERCKX B.: 'Channel characterization of indoor wireless personal area networks', *IEEE Trans. Antennas Propag.*, 2006, **54**, (11), pp. 3143–3150
- [13] MEDBO J., BERG J.E., HARRYSSON E.: 'Temporal radio channel variations with stationary terminal'. Proc. IEEE VTC2004-Fall, 2004, vol. 1, pp. 91–95
- [14] THOMA R., HAMPICKE D., RICHTER A., ET AL.: 'Identification of time-variant directional mobile radio channels', *IEEE Trans. Instrum. Meas.*, 2000, **49**, (2), pp. 357–364
- [15] 'Skycross inc', <http://www.skycross.com>, accessed February 2009
- [16] BULTITUDE R.: 'Methods for estimating and modeling consistency intervals, and the detection and simulation of changes on mobile radio channels'. COST 2100, TD(08) 424, Wroclaw, Poland, 2008
- [17] HERDIN M., BONEK E.: 'A MIMO correlation matrix based metric for characterizing non-stationarity'. Proc. IST Mobile and Wireless Communications Summit, Lyon, France, 2004
- [18] GEHRING A., STEINBAUER M., GASPARD I., GRIGAT M.: 'Empirical channel stationarity in urban environments'. Proc. Fourth European Personal Mobile Communications Conf. (EPMCC, 01), Vienna, Austria, 2001
- [19] YICK J., MUKHERJEE B., GHOSAL D.: 'Wireless sensor network survey', *Comput. Netw.*, 2008, **52**, (12), pp. 2292–2330
- [20] AKYILDIZ I.F., SU W., SANKARASUBRAMANIAM Y., CAYIRCI E.: 'A survey on sensor networks', *IEEE Commun. Mag.*, 2002, **40**, (8), pp. 102–114
- [21] GREENSTEIN L.J., MICHELSON D.G., ERCEG V.: 'Moment-method estimation of the Ricean K-factor', *IEEE Commun. Lett.*, 1999, **3**, (6), pp. 175–176
- [22] AKAIKE H.: 'Information theory and an extension of the maximum likelihood principle', in KOTZ S., JOHNSON N.L. (EDS.): 'Breakthroughs in statistics' (Springer, New York, 1992) pp. 610–624 (originally published in Proc. Int. Symp. Inf. Theory, Budapest, Hungary, 1973)
- [23] SCHUSTER U., BOLCSKEI H.: 'Ultrawideband channel modeling on the basis of information-theoretic criteria', *IEEE Trans. Wirel. Commun.*, 2007, **6**, (7), pp. 2464–2475
- [24] CHEN Y., BEAULIEU N.C.: 'Estimators using noisy channel samples for fading distribution parameters', *IEEE Trans. Commun.*, 2005, **53**, (8), pp. 1274–1277
- [25] BALAKRISHNAN N., KATERI M.: 'On the maximum likelihood estimation of parameters of weibull distribution based on complete and censored data', *Stat. Probab. Lett.*, 2008, **78**, (17), pp. 2971–2975
- [26] MOLISCH A.F.: 'Wireless communications' (IEEE Press, Wiley, Chichester, UK, 2005)
- [27] ALMERS P., BONEK E., BURR A., ET AL.: 'Survey of channel and radio propagation models for wireless MIMO systems', *EURASIP J. Wireless Commun. Netw.*, 2007, Article ID 19070